THE JOURNAL OF PHYSICAL CHEMISTRY A
A JOURNAL OF THE AMERICAN CHEMICAL SOCIETY

pubs.acs.org/JPCA

Article

Formation of the Elusive Silylenemethyl Radical ($HCSiH_2$; X^2B_2) via the Unimolecular Decomposition of Triplet Silaethylene (H_2CSiH_2; a^3A'')

Chao He, Aaron M. Thomas, Beni B. Dangi, Tao Yang, Ralf I. Kaiser,* Huan-Cheng Lee, Bing-Jian Sun, and Agnes H. H. Chang*

Cite This: *J. Phys. Chem. A* 2022, 126, 3347−3357

Read Online

ACCESS | Metrics & More | Article Recommendations | Supporting Information

ABSTRACT: We investigated the formation of small organosilicon molecules—potential precursors to silicon-carbide dust grains ejected by dying carbon-rich asymptotic giant branch stars—in the gas phase via the reaction of atomic carbon (C) in its ^3P electronic ground state with silane (SiH_4; X^1A_1) using the crossed molecular beams technique. The reactants collided under single collision conditions at a collision energy of 13.0 ± 0.2 kJ mol^{-1}, leading to the formation of the silylenemethyl radical ($HCSiH_2$; X^2B_2) via the unimolecular decomposition of triplet silaethylene (H_2CSiH_2; a^3A''). The silaethylene radical was formed via hydrogen migration of the triplet silylmethylene ($HCSiH_3$; X^3A'') radical, which in turn was identified as the initial collision complex accessed via the barrierless insertion of atomic carbon into the silicon−hydrogen bond of silane. Our results mark the first observation of the silylenemethyl radical, where previously only its thermodynamically more stable methylsilylidyne (CH_3Si; X^2A'') and methylenesilyl (CH_2SiH; X^2A') isomers were observed in low-temperature matrices. Considering the abundance of silane and the availability of atomic carbon in carbon-rich circumstellar environments, our results suggest that future astrochemical models should be updated to include contributions from small saturated organosilicon molecules as potential precursors to pure gaseous silicon-carbides and ultimately to silicon-carbide dust.

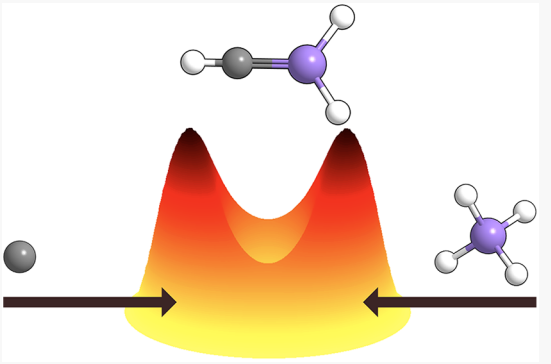

1. INTRODUCTION

Circumstellar envelopes (CSEs) of carbon-rich asymptotic giant branch (AGB) stars are host to a complex gas-phase chemistry that has required decades of interdisciplinary research effort to decode.[1] Besides the well-known combustion-like processes occurring near the stellar photosphere such as aromatic molecule formation by hydrogen-abstraction acetylene-addition[2−5] and hydrogen-abstraction-vinylacetylene-addition sequences,[6−8] the chemical and physical conditions within these envelopes are ideal for the production of silicon-carbide dust grains as signified by a unique absorption near 11.3 μm (885 cm^{-1}).[9,10] Approximately 90% of the silicon-carbide grains recovered from meteorites have been connected to formation processes in CSEs of low mass carbon-rich AGB stars;[11,12] recent dating of silicon-carbide grains revealed that in rare cases, these pre-solar materials can survive for up to a few billion years.[13] Following their formation in CSEs, and once incorporated in cold molecular clouds, these nanometer-sized grains can accumulate icy layers of a few hundred nanometers containing predominantly water (H_2O), methanol (CH_3OH), formaldehyde (H_2CO), carbon monoxide (CO), carbon dioxide (CO_2), methane (CH_4), and ammonia (NH_3).[14,15] These ices can be processed by the internal ultraviolet field present even deep inside molecular clouds and by energetic galactic cosmic rays leading to the synthesis of complex organic molecules often with biological significance such as urea [$(NH_2)_2CO$],[16,17] sugar-related molecules such as glycerol [$CHOH(CH_2OH)_2$],[18] (di)-phosphates,[19] aminoacids,[20−22] and even dipeptides.[23−26] Laboratory experiments have further suggested that silicon-carbide dust may also be linked to the formation of large fullerenes[27,28] and polycyclic aromatic hydrocarbons.[29,30] Despite their importance to circumstellar and interstellar chemistry, the elementary reactions leading to the formation these silicon-carbide grains remain elusive.

Gaseous molecules carrying silicon−carbon bonds in carbon-rich envelopes are considered the progenitors of silicon-carbide dust where at least eight molecules carrying a silicon−carbon bond are known to exist in the CSE of IRC +10216 (Scheme 1).[31−38] Systematic observations of carbon-

Received: March 16, 2022
Revised: May 2, 2022
Published: May 18, 2022

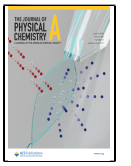

https://doi.org/10.1021/acs.jpca.2c01853
J. Phys. Chem. A 2022, 126, 3347−3357

Scheme 1. Molecules Carrying Silicon−Carbon Bonds Detected in the CSE of IRC+10216; Silicon, Carbon, Nitrogen, and Hydrogen Are Indicated in Purple, Gray, Blue, and White

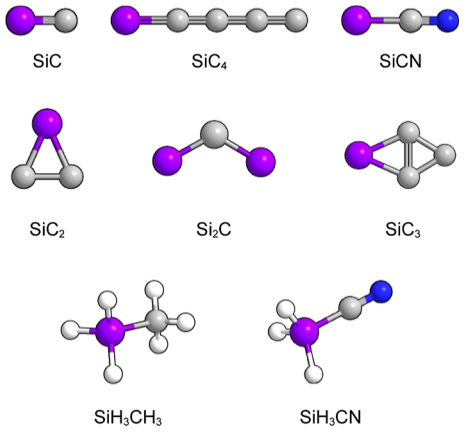

rich AGB stars discovered an anti-correlation between gaseous silicon dicarbide (c-SiC_2) abundances and the density of the envelopes[39] that models suggest could be explained by the nucleation of pure gaseous silicon carbide grains leading to increasingly stable clusters and eventually solids.[40,41] However, the inventory of gaseous molecules in CSEs is not limited to pure silicon-carbides. The presence of silylmethane (SiH_3CH_3) within IRC+10216 proposes that a chemistry involving saturated molecules such as methane (CH_4) and silane (SiH_4) could contribute to the initial formation of silicon-carbon bonds in CSEs as well. Despite this, the gas-phase characterization of small saturated organosilicon molecules formed from simple atomic and molecular precursors remains a work in progress for the (astro)chemistry and reaction dynamics communities.

A hitherto scarcely recognized pathway to silicon-carbides is the gas phase reaction of carbon atoms [$C(^3P)$] with silane (SiH_4), which has an abundance of 2.2×10^{-7} relative to molecular hydrogen in IRC+10216.[42,43] Early computational studies predicted that atomic carbon could insert into an Si−H bond of silane without an entrance barrier[44] as contrasted to the insertion of $C(^3P)$ into methane (CH_4), which has a 51 kJ mol^{-1} barrier in the entrance channel.[45] Lu et al. performed the first combined experimental and computational investigation of this reaction and proposed three triplet $CSiH_4$ intermediates to be involved in the formation of the products $CSiH_3$ and $CSiH_2$ with branching ratios of 60 versus 40% on the triplet potential energy surface.[46] Importantly, the molecular beam contained ground *and* electronically excited carbon atoms which complicates the interpretation of the experimental findings. Recently, Ranka et al. approached the $C(^3P/^1D)$−SiH_4 systems through a computational lens developing additional reaction pathways on the singlet potential energy surface and ultimately located an elusive C···SiH_4 van der Waals (vdW) complex in the entrance channel highlighting the possibility of a submerged barrier.[47] Considering the aforementioned experimental ambiguities, here, we present the results of crossed molecular beams experiments of solely ground-state carbon atoms $C(^3P)$ with silane (SiH_4; X^1A_1) in an attempt to untangle the reaction dynamics initiated on the triplet $CSiH_4$ surface. Merged with comprehensive electronic structure calculations, our data suggest that the carbon atom undergoes barrierless insertion into the silicon−hydrogen bond of silane resulting in a triplet $HCSiH_3$ collision complex leading ultimately to the doublet silylenemethyl ($HCSiH_2$) radical. These findings motivate continued research in the area of organosilicon chemistry and provide a well-founded chemical insight into the possible formation of small saturated silicon-carbides within carbon-rich CSEs as precursors to pure silicon-carbides and ultimately silicon-carbide dust.

2. METHODS

2.1. Experimental Section. The reaction of atomic carbon with silane (Voltaix; 99.9999%) was performed utilizing a crossed molecular beams machine at the University of Hawaii.[48,49] The carbon atoms were produced in their electronic ground state by ablation of a rotating graphite rod using the focused fourth harmonic of a Nd:YAG laser operating at a reduced output energy of 10 mJ per pulse.[50−55] The ablated carbon atoms were subsequently entrained in a pulsed beam of neon gas (99.999%; Specialty Gases of America), skimmed, and then velocity-selected using a four-slot chopper wheel rotating at 120 Hz. This part of the pulse was characterized by a peak velocity v_p of 1505 ± 10 m s^{-1} and a speed ratio S of 3.3 ± 0.1; note that under these experimental conditions, dicarbon (C_2) is also produced with the same beam properties.[56] A neat silane beam (v_p = 841 ± 10 m s^{-1}; S = 10.2 ± 0.3) was spatially and temporally aligned to intersect perpendicularly the carbon atom beam resulting in a nominal collision energy of 13.0 ± 0.2 kJ mol^{-1} and a center-of-mass angle (CM) of 56.1 ± 0.4° (Table 1). The reactively scattered products entered a triply differentially pumped universal detector rotatable in the plane defined by the reactant beams. The products were ionized at 80 eV and filtered according to their mass-to-charge (m/z) ratio using a quadrupole mass spectrometer. Ions of the desired m/z impinged upon an aluminum target floated at a negative voltage of 25 kV; this generated a cascade of secondary electrons that struck an aluminum coated scintillator whose photons were registered by a photomultiplier tube. The resulting signal was collected by a multichannel scaler in discrete bins according to the time of arrival to produce a time-of-flight (TOF) spectrum. The laboratory data are forward-convoluted to the CM frame and the resulting CM translational energy $P(E_T)$ and angular $T(\theta)$ flux distributions are analyzed to inform the reaction dynamics.[57,58] Errors of the $P(E_T)$ and $T(\theta)$ functions are determined within the 1σ error

Table 1. Peak Velocities (v_p) and Speed Ratios (S) of the Carbon (C), Dicarbon (C_2), and Silane (SiH_4) Beams along with the Corresponding Collision Energies (E_C) and CMs (Θ_{CM})

beam	v_p (m s^{-1})	S	E_C (kJ mol^{-1})	Θ_{CM} (deg)
SiH_4 (X^1A_1)	841 ± 10	10.2 ± 0.3		
C (^3P)	1505 ± 10	3.3 ± 0.1	13.0 ± 0.2	56.1 ± 0.4
C_2 ($X^1\Sigma_g^+/a^3\Pi_u$)	1505 ± 10	3.3 ± 0.1	20.4 ± 0.2	36.7 ± 0.4

https://doi.org/10.1021/acs.jpca.2c01853
J. Phys. Chem. A 2022, 126, 3347−3357

limits of the accompanying LAB angular distribution while maintaining a good fit of the laboratory TOF spectra.

2.2. Computational. On both adiabatic triplet and singlet potential energy surfaces of $CSiH_4$, the geometries of various $CSiH_4$, $CSiH_3$, and $CSiH_2$ isomers and transition states are optimized, and the 1-D barrierless reaction paths are mapped out via IRC (intrinsic reaction coordinate calculation) by coupled cluster[59,60] CCSD/cc-pVTZ calculations. The complete basis set limits,[61] CCSD(T)/CBS energies for stationary points, are then obtained by extrapolating the CCSD(T)/cc-pVDZ, CCSD(T)/cc-pVTZ, and CCSD(T)/cc-pVQZ energies, with CCSD/cc-pVTZ zero-point energy corrections. The accuracy of these CCSD(T)/CBS energies is within 8 kJ mol^{-1}.[62] GAUSSIAN09 programs[63] are facilitated in coupled cluster calculations. The minimum energy crossing point between the triplet (^{3}**i1**) and singlet (^{1}**i1**) silylmethylene is located with the CPMCSCF/TZVPP by employing MOLPRO,[64] and the CCSD(T)/CBS energy is also computed.

3. RESULTS

3.1. Laboratory Frame. Carbon atoms in their electronic ground state (^{3}P) underwent reactive collisions with silane (SiH_4) at a collision energy of 13.0 ± 0.2 kJ mol^{-1}; distinct TOF spectra were recorded at mass-to-charge ratios m/z = 43 ($CSiH_3^+$) and m/z = 42 ($CSiH_2^+$). The presence of singly ionized carbon dioxide (CO_2^+) in the detector prevented the collection of TOFs at m/z = 44 of ionized $^{13}C^{28}SiH_3/^{12}C^{29}SiH_3$ or $^{12}C^{30}SiH_2$ formed via atomic or molecular hydrogen loss(es) and/or as an adduct ($^{12}C^{28}SiH_4$). The TOF spectra (Figure 1a) recorded at m/z = 43 and m/z = 42 were superimposable (Figure 1b) and therefore have a common origin owing to the atomic hydrogen loss channel(s): C (12 amu) + SiH_4 (32 amu) → $CSiH_3$ (43 amu) + H (1 amu) (reaction 1); signal at m/z = 42 stems from dissociative electron impact ionization of the neutral $CSiH_3$ species within the ionizer. Given that the multichannel nature of this reaction had been both observed and predicted previously,[46,47] we extracted the full laboratory angular distribution for both $CSiH_3^+$ (m/z = 43) [Figure 2 (top)] and $CSiH_2^+$ (m/z = 42) [Figure 3 (left)] by recording TOF spectra at discrete angles in 5° intervals. Up to 7.3 × 10^5 and 6.9 × 10^5 TOF spectra were recorded at m/z = 43 [Figure 2 (bottom)] and m/z = 42 [Figure 3 (right)] at each angle, respectively. These data were then integrated and normalized to produce the laboratory angular distributions presented in Figures 2 (top) and 3 (left).

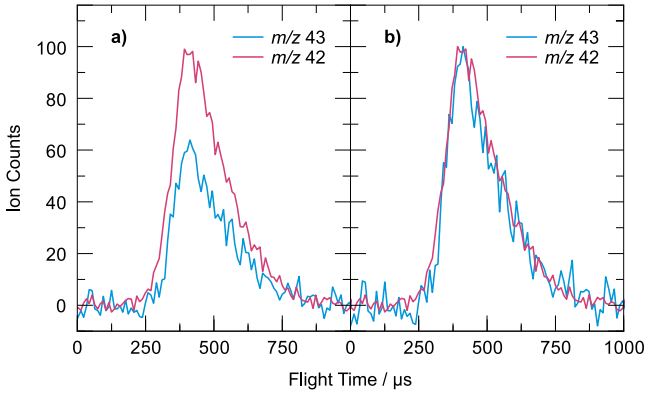

Figure 1. TOF spectra recorded at the CM for m/z = 43 ($CSiH_3^+$) and m/z = 42 ($CSiH_2^+$). The left and right panels depict raw and normalized TOF spectra, respectively.

$$C + SiH_4 \rightarrow CSiH_3 + H \quad (1)$$

$$C + SiH_4 \rightarrow CSiH_2 + H_2 \quad (2)$$

$$C_2 + SiH_4 \rightarrow C_2SiH_2 + H_2 \quad (3)$$

The resulting distributions of the ion counts of $CSiH_3^+$ (m/z = 43) and $CSiH_2^+$ (m/z = 42) are both very broad and asymmetric, covering a range of more than 50° in the laboratory frame; each distribution peaks nearly 10° below the CM angle of the C(^{3}P)−SiH_4 system (Table 1). Both distributions terminate at 69° due to limitations in the machine configuration that prevents scanning at larger angles. To account for these broad and asymmetric distributions, a second reaction channel arising from dicarbon (C_2)—a known byproduct of graphite ablation[56,65]—and silane was required. In the selected part of the beam, the dicarbon (C_2) to atomic carbon (C) ratio of 0.5 ± 0.05:1 was determined, that is, a fraction of about 33%. The chemical dynamics of the C_2−SiH_4 system were untangled earlier in our laboratory;[66] these experiments revealed the existence of a single reaction channel leading to $C_2{}^{28}SiH_2$ isomer(s) (54 amu) (hereafter: C_2SiH_2) along with molecular hydrogen (2 amu) (reaction 3). Here, acceptable fits of the signal obtained at m/z = 43 and m/z = 42 could be obtained by the inclusion of the C_2−SiH_4 reactions that lead to molecular hydrogen loss products of 55 ($C_2H_2{}^{29}Si$)/54 ($C_2H_2{}^{28}Si$) amu, respectively, with fragments from dissociative electron impact ionization arising at m/z = 43 and m/z = 42. This gives a maximum near the CM angle of the C_2−SiH_4 system of 36.7 ± 0.4° (Figures 2 and 3). At higher laboratory angles, the reactive scattering data could be fit with a single channel, namely, C (12 amu) + SiH_4 (32 amu) → $CSiH_3$ (43 amu) + H (1 amu), resulting in a nearly symmetric distribution about CM angle of 56.1 ± 0.4°. The CM functions used to fit the data recorded at m/z = 43—discussed in the next section—could also be used to fit the data recorded at m/z = 42. Most importantly, these findings support the carbon versus hydrogen atom exchange pathway, but they do not support the formation of molecular hydrogen loss products where inclusion of a molecular hydrogen loss product channel results in extremely narrow TOF distributions.

3.2. Center-of-Mass Frame. To elucidate the chemical dynamics of the bimolecular reactions of the C−SiH_4 system, the experimental data were transformed from the laboratory into the CM reference frame to obtain the CM translational energy $P(E_T)$ and angular $T(\theta)$ flux distributions (Figure 4).[67]

3.2.1. m/z = 43. The TOFs and laboratory angular distribution at m/z = 43 (Figure 2) could be replicated via a two-channel fit: (i) the reaction C (12 amu) + $^{28}SiH_4$ (32 amu) → $C^{28}SiH_3$ (43 amu) + H (1 amu) (reaction 1), and (ii) dissociative electron impact ionization of the m/z = 55 ($C_2{}^{29}SiH_2^+$) formed in the reaction C_2 + $^{29}SiH_4$ → $C_2{}^{29}SiH_2$ (55 amu) + H_2 (reaction 3). The overall branching ratios for the channels (i) and (ii) are 67 ± 5 and 33 ± 3%, respectively, with the CM functions of the molecular hydrogen loss channel for the C_2−SiH_4 system extracted from Rettig et al.[66] For the dominant channel, (i) the reaction C (12 amu) + $^{28}SiH_4$ (32 amu) → $C^{28}SiH_3$ (43 amu) + H (1 amu) (reaction 1), the best-fit $P(E_T)$ reveals that the maximum translational energy for the hydrogen atom loss channel leading to $CSiH_3$ product(s) is 105 ± 15 kJ mol^{-1}; this corresponds to the

https://doi.org/10.1021/acs.jpca.2c01853
J. Phys. Chem. A 2022, 126, 3347−3357

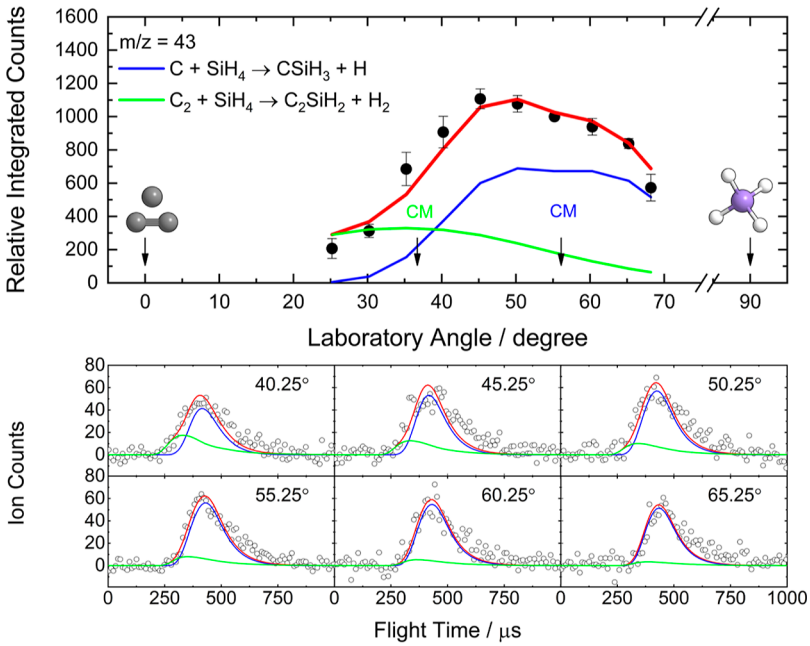

Figure 2. Laboratory angular distribution (top) and TOF spectra (bottom) recorded at m/z = 43 for the reaction of atomic carbon and dicarbon with silane. The data were fit with two channels (i) ^{12}C (12 amu) + $^{28}SiH_4$ (32 amu) → $^{12}C^{28}SiH_3$ (43 amu) + H (1 amu) (blue), (ii) dissociative electron impact ionization of the m/z = 55 ($^{12}C_2{}^{29}SiH_2^+$) formed in the reaction $^{12}C_2$ (24 amu) + $^{29}SiH_4$ (33 amu) → $^{12}C_2{}^{29}SiH_2$ (55 amu) + H_2 (2 amu) (green). The black circles depict the experimental data, colored lines the fits (red corresponding to the total fit), and error bars the 1s standard deviation. Colors of the atoms: silicon, purple; carbon, gray; and hydrogen, white.

total energy available E_{avail} to the reaction products (Figure 4A). The $P(E_T)$ distribution carries a most probable E_T of 22 ± 3 kJ mol^{-1}, while on average, 34 ± 5 kJ mol^{-1} are apportioned to the translational degrees of freedom representing 33 ± 7% of the available energy. The relatively low fraction of energy used for the translation of nascent atomic hydrogen loss products along with the away-from-zero translational energy peaking of the $P(E_T)$ for each channel suggests the reaction proceeds indirectly via $CSiH_4$ intermediate(s) decomposing via tight exit transition state(s). For products formed without rovibrational excitation, the maximum energy cutoff of 105 ± 15 kJ mol^{-1} is representative of the reaction (Δ_rG) and collision energies through $E_{avail} = E_C - \Delta_rG$. Therefore, a reaction energy (Δ_rG) of −92 ± 15 kJ mol^{-1} can be derived based on the known experimental collision energy (E_C) of 13.0 ± 0.2 kJ mol^{-1}. The best-fit CM angular flux distribution [$T(\theta)$] reveals that the reaction products are scattered at all angles (Figure 4B). Furthermore, the $T(\theta)$ distribution is symmetric about the 90° minimum which is characteristic of indirect reaction dynamics owing to $CSiH_4$ intermediate(s) that persists for several rotational periods such that the memory of the reactant trajectories is lost prior to dissociation to $CSiH_3$ plus atomic hydrogen. The minimum at 90° can arise from geometrical constraints in the exit channel where the hydrogen atom is emitted in the rotational plane of the decomposing transition state.[68,69] These findings are also compiled in the flux contour map, which depict the reactively scattering products flux intensity as a function of the center-of-mass scattering angle (θ) and product velocity (u), providing the detailed messages on the reactive scattering process (Figure 4C).[69]

3.2.2. m/z = 42. The two-channel fit could reproduce the experimental data at m/z = 42 [Figure 3 (top)] via channels i and ii along with branching ratios of 82 ± 5 and 18 ± 8%, respectively [Figure 3 (top)]. Finally, we also explored if a third channel—^{12}C (12 amu) + $^{28}SiH_4$ (32 amu) → $^{12}C^{28}SiH_2$ (43 amu) + H_2 (1 amu) (magenta; reaction 2) with CM functions stemmed from Lu et al.[46]—could be implemented [Figure 3 (bottom)]. The overall branching ratios for the channels i, ii, and iii in the three-channel fit are 70 ± 5, 16 ± 3, and 14 ± 4%, respectively. The fits suggest that the channels ii and iii have only minor contributions—if at all [Figure 3 (bottom)].

4. DISCUSSION

Our experiments reveal that the carbon atom reacts exoergically (−92 ± 15 kJ mol^{-1}) with silane to form $CSiH_3$ via atomic hydrogen loss in an indirect reaction involving $CSiH_4$ reaction intermediate(s) (Figures 5 and S1−S6 and Tables S1−S2). To understand the reaction mechanism underlying the experimental data, we introduce a comparison with electronic structure calculations to determine which structural isomers are produced. For completeness, we have considered four $CSiH_3$ (**p1**−**p4**) and three $CSiH_2$ isomers (**p5**−**p7**) as possible reaction products. The $CSiH_3$ isomers are the doublets silylmethylidyne [^{2}**p1** ($CSiH_3$; X^2A'')], silylenemethyl [^{2}**p2** ($HCSiH_2$; X^2B_2)], methylenesilyl [^{2}**p3** (H_2CSiH; X^2A')], and methylsilylidyne [^{2}**p4** (CH_3Si; X^2A'')]. Each of the three $CSiH_2$ isomers can be formed on both the singlet (Figure 5b) and triplet surfaces (Figure 5a). The singlet silylenecarbene [^{1}**p5** ($CSiH_2$; X^1A_1)] and silylidene [^{1}**p7** (H_2CSi; X^1A_1)] isomers are stabilized by a carbon−silicon π-bond giving rise to carbene and silylene moieties with C_{2v} symmetry, while silaacetylene [^{1}**p6** (HCSiH; X^1A')] is planar and supported by a Si−C triple bond of only 1.653 Å. The triplet $CSiH_2$ isomer ^{3}**p7** (H_2CSi; a^3A_2) has two unpaired electrons on the silicon atom, while the ^{3}**p5** ($CSiH_2$; a^3A'') and ^{3}**p6** (HCSiH; a^3A'') diradicals have an unpaired electron on both the carbon and silicon atom. Considering the experimentally derived

https://doi.org/10.1021/acs.jpca.2c01853
J. Phys. Chem. A 2022, 126, 3347−3357

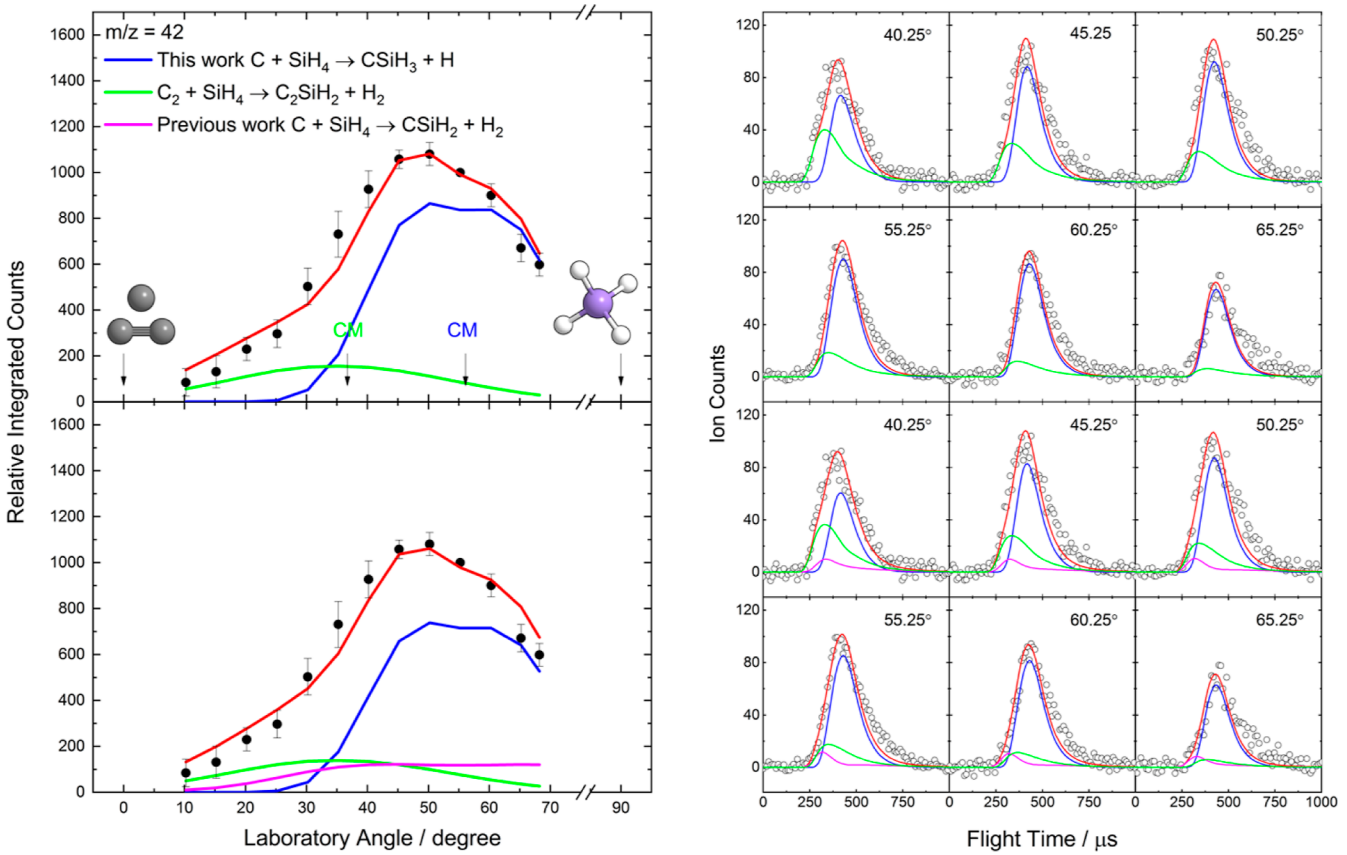

Figure 3. Laboratory angular distribution (left) and TOF spectra (right) recorded at m/z = 42 for the reaction of atomic carbon and dicarbon with silane. The data were fit with two channels (top) and with three channels (bottom): (i) ^{12}C (12 amu) + ^{28}SiH$_4$ (32 amu) → ^{12}C^{28}SiH$_3$ (43 amu) + H (1 amu) (blue), (ii) dissociative electron impact ionization of the m/z = 55 (^{12}C$_2$^{29}SiH$_2^+$) formed in the reaction ^{12}C$_2$ (24 amu) + ^{29}SiH$_4$ (33 amu) → ^{12}C$_2$^{29}SiH$_2$ (55 amu) + H$_2$ (2 amu) (green) with CM functions derived from A. Rettig et al. (*J. Phys. Chem Lett.*, **2021**, *12*, 10768−10776), and (iii) ^{12}C (12 amu) + ^{28}SiH$_4$ (32 amu) → ^{12}C^{28}SiH$_2$ (43 amu) + H$_2$ (1 amu) (magenta) with CM functions from Lu et al. (*J. Chem. Phys.*, **2008**, *129*, 164304). The black circles depict the experimental data, colored lines the fits (red corresponding to the total fit), and error bars the 1s standard deviation. Colors of the atoms: silicon, purple; carbon, gray; and hydrogen, white.

energetics of the atomic hydrogen loss channel (−92 ± 15 kJ mol^{-1}) and the theoretically computed reaction energies of the four CSiH$_3$ isomers (**p1**−**p4**), the experiments and computations can be reconciled by suggesting that at least the ^{2}**p2** + H channel, with a computed reaction energy of −98 ± 4 kJ mol^{-1}, is representative of the reaction products. The formation of either ^{2}**p3** (H$_2$CSiH; X^{2}A′) or ^{2}**p4** (CH$_3$Si; X^{2}A″) is too exoergic, and ^{2}**p1** (CSiH$_3$; X^{2}A″) is energetically inaccessible at our experimental collision energy of 13.0 ± 0.2 kJ mol^{-1}.

The computations predict that the reaction of ground-state atomic carbon C(^{3}P) with silane (SiH$_4$) commences on the attractive triplet surface forming a vdW complex 1 kJ mol^{-1} below the energy of the separated reactants (Figure S5). Similar to Ranka et al.,[47] we were unable to locate a transition state connecting this complex to any CSiH$_4$ intermediates and thus conclude that the triplet vdW complex is metastable at most and that the insertion of atomic carbon into one of the four Si−H bonds to form silylmethylene (HCSiH$_3$; ^{3}**i1**) is essentially a barrierless process. The silylmethylene intermediate ^{3}**i1**, despite holding two unpaired electrons on the carbon atom, is relatively low-lying (345 kJ mol^{-1}) and can access several reaction outcomes. First, unimolecular decomposition via elimination of molecular hydrogen from the silyl group forms *trans*-silaacetylene (HCSiH; ^{3}**p6**) via a barrier of 238 kJ mol^{-1}. Products ^{2}**p1** (CSiH$_3$) and ^{2}**p2** (HCSiH$_2$) can be formed by the barrierless elimination of atomic hydrogen from the methylidyne and silyl group, respectively. Second, a hydrogen atom can migrate from the silicon to the carbon atom via a barrier located 180 kJ mol^{-1} below the reacts to form H$_2$CSiH$_2$ (^{3}**i2**). Intermediate ^{3}**i2** can dissociate to products ^{3}**p5** or ^{3}**p7**, respectively, by the elimination of molecular hydrogen from its methylene (CH$_2$) or silylene (SiH$_2$) groups, respectively; alternatively, the elimination of molecular hydrogen sourced from both carbon and silicon centers forms ^{3}**p6** via a transition state 53 kJ mol^{-1} above the products. Furthermore, atomic hydrogen loss products can be accessed from ^{3}**i2** with ejection from the methylene group yielding ^{2}**p2** over a relatively loose transition state located 5 kJ mol^{-1} above the product channel; hydrogen atom emission from the silylene group is a barrierless process and results in ^{2}**p3**. Third, yet another hydrogen shift from the silylene group of ^{3}**i2** to the carbon atom results in methylsilylene (H$_3$CSiH; ^{3}**i3**), the most stable intermediate on the triplet surface. Four products are accessible from ^{3}**i3**: ^{3}**p6**, ^{3}**p7**, ^{2}**p3**, and ^{2}**p4** by the elimination of molecular (^{3}**p6**, ^{3}**p7**) and atomic hydrogen (^{2}**p3**, ^{2}**p4**).

Following the initial insertion step, ^{3}**i1** can undergo intersystem crossing (ISC) to the singlet surface accessing ^{1}**i1** in which both electrons are paired at the carbon atom, thus representing a singlet carbene. On the singlet surface,

https://doi.org/10.1021/acs.jpca.2c01853
J. Phys. Chem. A 2022, 126, 3347−3357

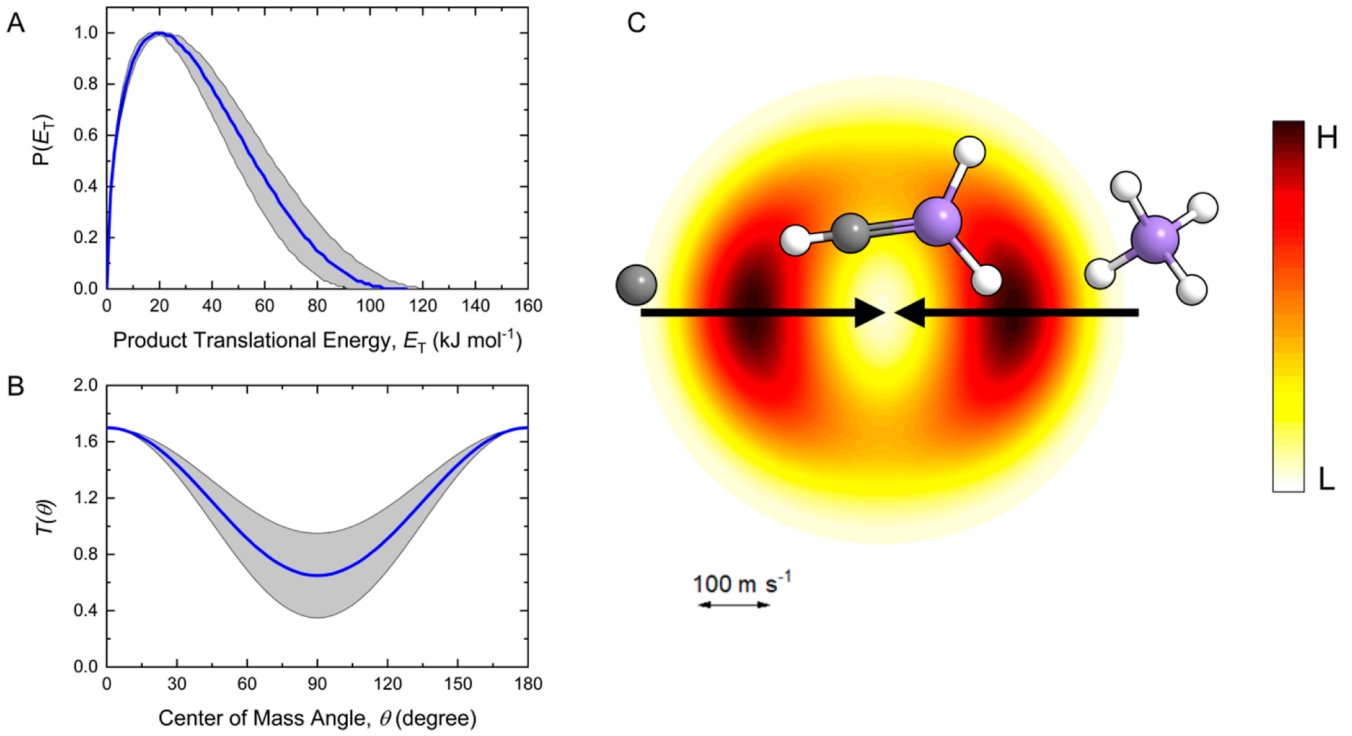

Figure 4. CM translational energy flux distribution (A), CM angular flux distribution (B), and the top view of the flux contour map (C), leading to the formation of silylenemethyl radical. Shaded areas indicate the acceptable upper and lower error limits, while the blue solid lines define the best fits. The flux contour map represents the flux intensity of the reactively scattered heavy products as a function of the CM scattering angle (θ) and product velocity (u). The color bar manifests the flux gradient from high (H) intensity to low (L) intensity. Colors of the atoms: silicon, purple; carbon, gray; hydrogen, white.

analogues of the triplet intermediates H_2CSiH_2 (^{3}**i2**) and H_3CSiH (^{3}**i3**) exists with ^{1}**i2** and ^{1}**i3** accessible via hydrogen migration. These intermediates are stabilized by 545 and 526 kJ mol^{-1}, respectively, relative to the C(^{3}P) plus SiH_4 reactants. At the CCSD/cc-pVTZ level, we locate a ^{1}**i1**−^{1}**i2** transition state with an energy slightly higher than ^{1}**i1**, as identified by Bartlett and co-workers.[47] However, the refined CCSD(T)/CBS energy of this transition state indicates that it is more stable than ^{1}**i1** and hence the electronic structure calculations suggest that silylmethylene is metastable on the singlet potential energy surface. The doublet products accessed from the singlet intermediates are formed exclusively by barrierless dissociation via hydrogen atom emission. Isomer ^{2}**p2** ($HCSiH_2$) can be accessed by hydrogen emission from the silyl group of ^{1}**i1** or from the methylene group of ^{1}**i2**. Cleavage of a Si−H bond in ^{1}**i2** yields ^{2}**p3** (H_2CSiH). In ^{1}**i3**, breaking of the silylidyne bond results in ^{2}**p4** (H_3CSi); cleavage of the C−H bond forms ^{2}**p3**. The singlet products ^{1}**p5**, ^{1}**p6**, and ^{1}**p7** are formed via molecular hydrogen loss with each involving a tight exit transition state. ^{1}**p5** can be formed by dissociation of ^{1}**i1** or ^{1}**i2** via Si−H or C−H bond fission, respectively. Lastly, the *trans*-silaacetylene ^{1}**p6** can be formed by molecular hydrogen loss from any of intermediates ^{1}**i1**, ^{1}**i2**, or ^{1}**i3**, whereas silylidene ^{1}**p7** can only be formed by the dissociation of ^{1}**i2** or ^{1}**i3**. A barrier from ^{1}**i1** to ^{1}**i2** was located at the CCSD/cc-pVTZ level of theory but vanishes at the CCSD(T)/CBS level. Therefore, we may conclude that ^{1}**i1** is metastable and rearranges rapidly to ^{1}**i2** rather than decomposing to ^{1}**p5**, ^{2}**p2**, and/or ^{1}**p6**.

With the identification of at least the ^{2}**p2** ($HCSiH_2$; X^2B_2) isomer silylenemethyl through atomic hydrogen loss, we are merging now the experimental and computational data in an attempt to propose the underlying reaction dynamics. For this, it is helpful to reduce the complex potential energy surface (Figure 5) to a reduced surface by eliminating the unobserved molecular hydrogen loss products and also pathways involving transition states which are higher than our collision energy of 13.0 ± 0.2 kJ mol^{-1}. This reduced surface is presented in Figure 6. ^{2}**p2** ($HCSiH_2$; X^2B_2) can be formed on the triplet surface via hydrogen atom emission from the silyl group of ^{3}**i1** or by C−H bond rupture in ^{3}**i2**. On the singlet surface, both ^{1}**i1** and ^{1}**i2** can also undergo unimolecular decomposition via loose exit transition states leading to ^{2}**p2** ($HCSiH_2$; X^2B_2). Considering that the CM translational energy distribution peaks away from zero translational energy, at least one of the exit channels should be reflected in a transition state located above the energy of the separated products, that is, the transition state involved in the unimolecular decomposition of ^{3}**i2**. Consequently, at least one channel involves the reaction sequence ^{3}**i1** → ^{3}**i2** → ^{2}**p2** + H and hence a hydrogen shift from the silicon to the carbon atom and existence of triplet silaethylene (^{3}**i2**). Thus, the lifetime of ^{3}**i1** has to be sufficiently long enough to allow this hydrogen migration to occur on the triplet surface.

Our experimental results stand in contrast to those obtained by Lu et al. who observed strongly exoergic reaction products CH_3Si (^{2}**p4**) and H_2CSi (^{3}**p7**) via atomic and molecular hydrogen loss pathways, respectively.[46] Besides, the theoretical calculations for the C(^{3}P) + SiH_4 reaction were also performed and suggested the dominant hydrogen atom loss channel along with the minor molecular hydrogen loss channel.[47,70] The branching ratio is found to be about 1.66,[70] which is very

https://doi.org/10.1021/acs.jpca.2c01853
J. Phys. Chem. A 2022, 126, 3347−3357

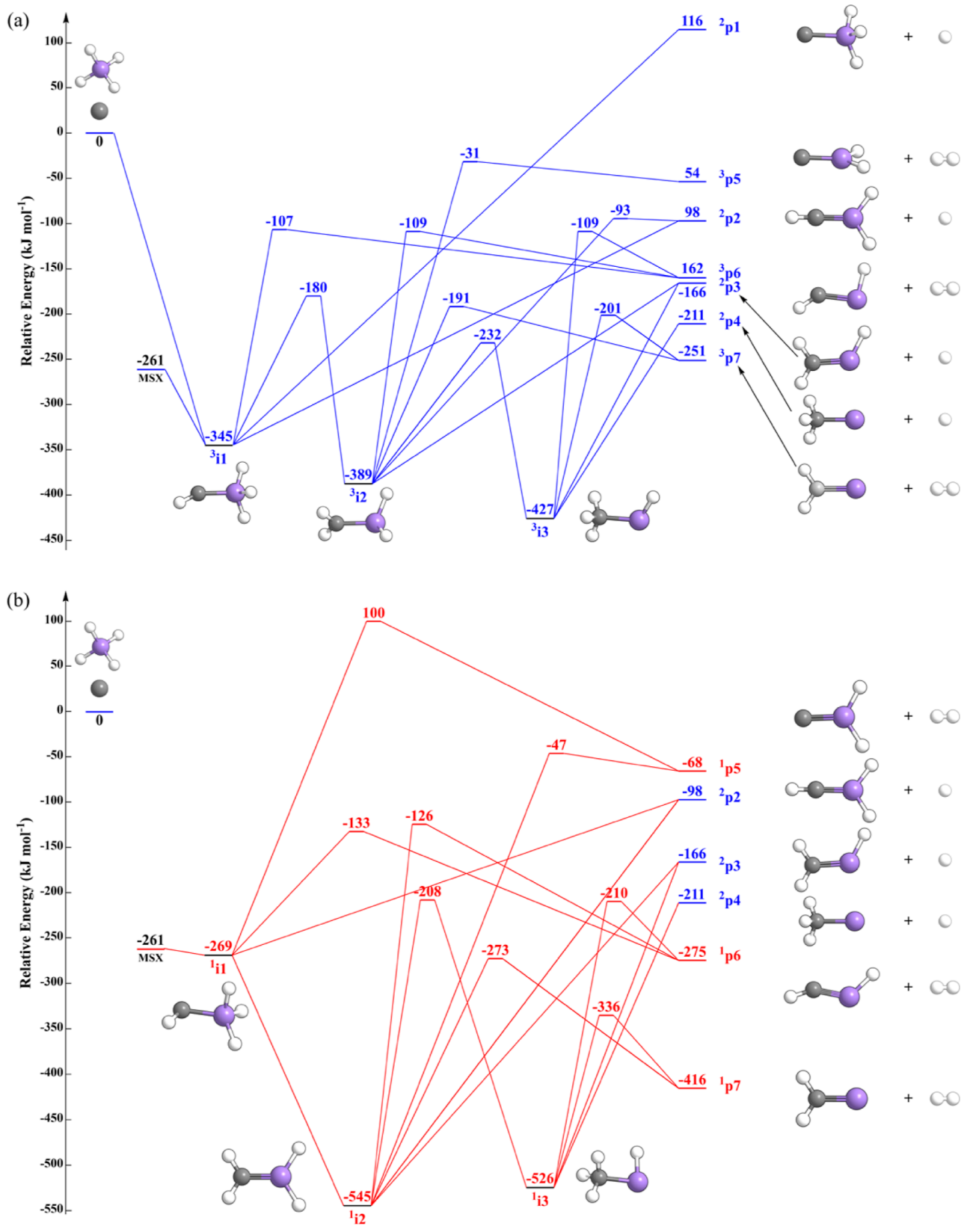

Figure 5. Pathways on the triplet (a) and singlet (b) accessed by the $C(^3P) + SiH_4(X^1A_1)$ reaction leading to $CSiH_3$ and $CSiH_2$ reaction products. Energies are given in kJ mol^{-1} and are relative to the reactants, $C(^3P) + SiH_4$ (X^1A_1). Singlet and triplet pathways and product channels are colored red and blue. MSX is the ^{3}**i1**−^{1}**i1** minimum energy crossing point (Figure S5).

comparable with the experimentally estimated value of 1.5 reported by Lu et al. One possibility for this difference could owe to the presence of electronically excited carbon atoms. Lu et al. produced ground and electronically excited (^{1}D) carbon atoms by electrical discharge of CO/He or CO/H_2 mixtures, whereas our beam consists of carbon atoms solely in their

https://doi.org/10.1021/acs.jpca.2c01853
J. Phys. Chem. A 2022, 126, 3347−3357

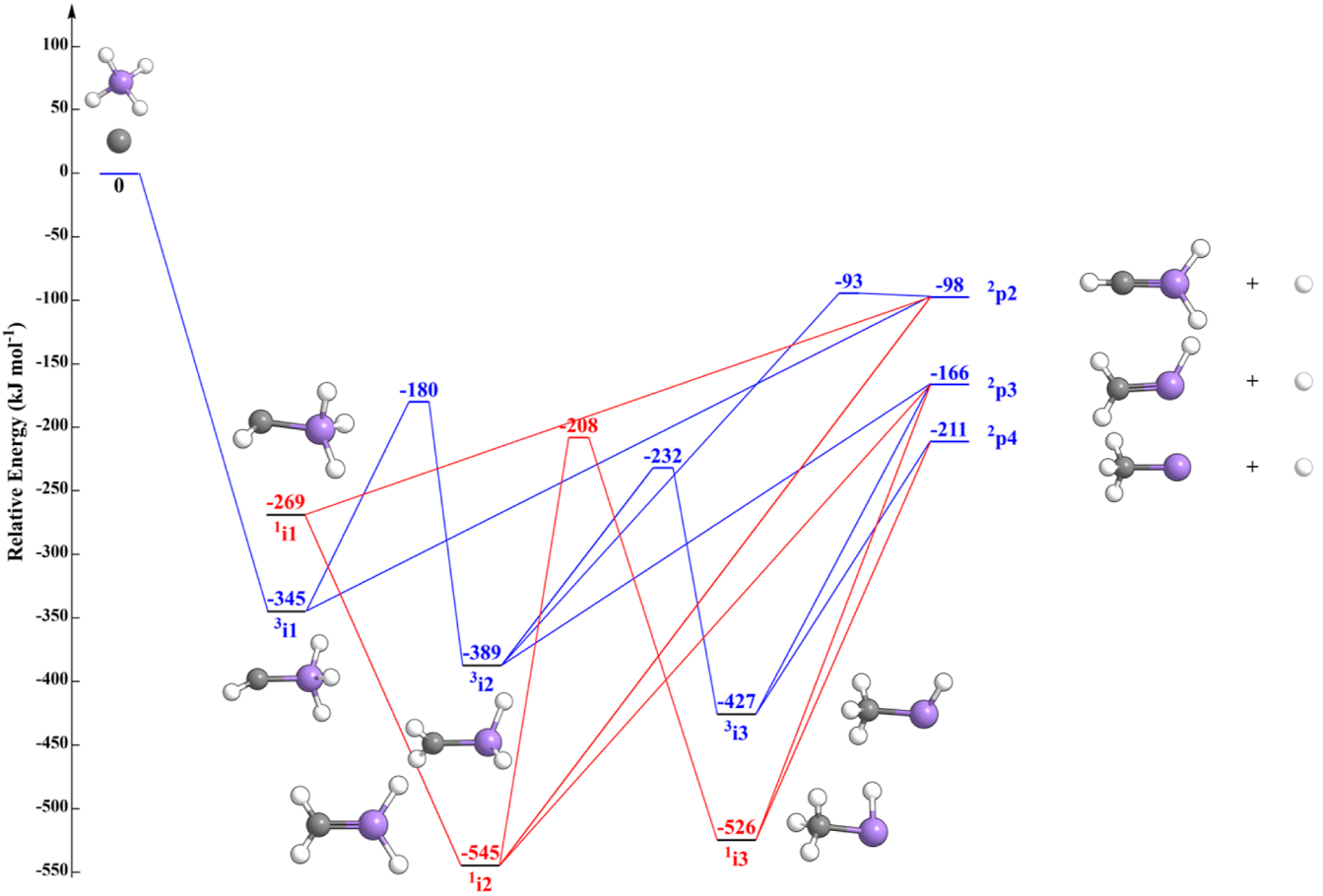

Figure 6. Simplified surface along with $C(^3P)$ + $SiH_4(X^1A_1)$ reaction pathways leading to atomic hydrogen loss products only. Energies are given in kJ mol^{-1} and are relative to the reactants, $C(^3P)$ + SiH_4 (X^1A_1). Singlet and triplet pathways and product channels are colored red and blue.

ground ^3P state. Incidentally, the ^1D state lies 122 kJ mol^{-1} above the ground state[71] and could potentially account for the energy gap in the observed $CSiH_3$ product channels, that is, between ^{2}**p2** (−98 ± 4 kJ mol^{-1}) and ^{2}**p4** (−211 ± 4 kJ mol^{-1}). If not properly accounted for, the presence of electronically excited reactants will adversely affect the interpretation of the reactive scattering data. As a matter of fact, the photoionization efficiency curves recorded by Lu et al. detected $C(^1D)$, but the contribution to the reactive scattering signal was ignored. Insertion of $C(^1D)$ into the silicon−hydrogen bond of silane forms intermediate ^{1}**i1** that isomerizes to ^{1}**i2** on the singlet surface. In this scenario, the excess energy carried into the reaction coordinate by the ^1D excited state will appear as product translational energy, thereby affecting the interpretation of reaction energies, structural isomers, and ultimately reaction pathways. The involvement of the singlet surface could also account for the fact that Lu et al. observed the molecular hydrogen channel, which was not detected in our experiments; this in turn might propose that our reaction takes place on the triplet surface and does not involve ISC.

Lastly, we note that silane (SiH_4), a group 14 tetrahydride, has undergone careful studies of reactive collision in the gas phase with $Si(^3P)$[72] and $Ge(^3P)$ as well.[73] The effects of the heavy atoms and the increased bond lengths they afford to molecular geometry are very apparent in structures accessed by these reactions. All $CSiH_4$ reaction intermediates are stabilized by covalent bonds unlike some Si_2H_4 and $GeSiH_4$ molecules that carry single and double hydrogen bridges and hence multicenter bonds. Experiments observed that in the $Si(^3P)$ + SiH_4 system, only the singlet disilavinylidene ($SiSiH_2$) molecule—the silicon analogue of vinylidene (CCH_2)—is formed by the emission of molecular hydrogen. Similarly, experimental studies of the $Ge(^3P)$−SiH_4 system identified the singlet dibridged germaniumsilylene [$Ge(\mu$-$H_2)Si$] molecule as the nascent reaction product. Notably, the $Si(^3P)$ and $Ge(^3P)$ reactions with silane follow reaction coordinates underpinned by crossing from the triplet to singlet surfaces, whereas the $C(^3P)$ + SiH_4 reaction occurred explicitly on the triplet surface. These differences are likely due the heavy atom effect induced by the presence of silicon and germanium atoms.

5. CONCLUSIONS

Using the crossed molecular beams technique, we investigated the reaction of ground-state carbon atoms $C(^3P)$ with silane (SiH_4) under single-collision conditions. Our experimental data suggest the formation of silylenemethyl ($HCSiH_2$; X^2B_2) via the unimolecular decomposition of triplet silaethylene (H_2CSiH_2; a^3A''). Triplet silaethylene was formed via hydrogen migration within triplet silylmethylene ($HCSiH_3$; X^3A''), which in turn was identified as the initial collision complex accessed via barrierless insertion of atomic carbon into the silicon−hydrogen bond of silane. Our results mark the first observation of the silylenemethyl radical where only its more stable isomers methylsilylidyne (CH_3Si) and methylenesilyl (H_2CSiH) had been detected previously in irradiated methane−silane ice mixtures;[74,75] methylsilylidyne was also

https://doi.org/10.1021/acs.jpca.2c01853
J. Phys. Chem. A 2022, 126, 3347−3357

observed in a previous crossed molecular beams experiment.[46] The silylenemethyl radical is isoelectronic with the vinyl (H_2CCH) radical yet remains distinct in its molecular geometry. The vinyl radical is planar (C_S) and the unpaired electron is stabilized in a sp^2 hybridized orbital located at the C−H group (Figure 7). Replacement of a single carbon atom

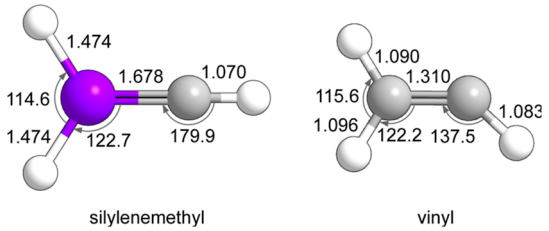

Figure 7. Molecular geometries for the isoelectronic silylenemethyl ($HCSiH_2$) and vinyl ($HCCH_2$) radicals in their respective $^2B_2$ and $^2A'$ electronic ground states.

with silicon and its larger valence orbitals ultimately influences hybridization efficiency in the resulting silylenemethyl radical.[76−78] In this configuration, the carbon atom is connected to silicon by a single σ and π bond; however, it is not sp^2 hybridized. Bonding at the carbon atom adopts sp character, resulting in a Si−C bond length of 1.678 Å midway between the double and triple bond lengths observed in organosilicon molecules. Consequently, the unpaired electron is stabilized in a nonbonding p orbital on the carbon atom perpendicular to the silicon−carbon axis.

Although $CSiH_3$ isomers have not been detected in the CSEs of carbon-rich AGB stars, the availability of atomic carbon and silane in these environments along with the presence of saturated molecules carrying silicon-carbon bonds such as silylmethane (SiH_3CH_3) suggest that the silylenemethyl ($HCSiH_2$; X^2B_2) radical should be present within CSEs such as IRC+10216. Therefore, silylenemethyl could be an important precursor to pure silicon-carbide gaseous molecules such as silicon carbide (SiC). Contemporary models of carbon-rich CSEs however treat silicon-carbide dust as the sole consequence of Si_xC_y nucleation and neglect the obvious chemistry involving abundant chemical species in these envelopes such as carbon and silane. Our results suggest that these models must be updated to include contributions from organosilicon molecules as potential precursors to pure gaseous silicon-carbide molecules and ultimately to silicon-carbide dust as demonstrated in the present study.

■ ASSOCIATED CONTENT

Supporting Information

The Supporting Information is available free of charge at https://pubs.acs.org/doi/10.1021/acs.jpca.2c01853.

Comparison of CM functions between our study and Lu et al.; CCSD/cc-pVTZ optimized geometries of $CSiH_3$ and $CSiH_2$ isomers along with their bond lengths (angstroms), bond angles, and ground-state symmetry; CCSD/cc-pVTZ optimized structures of singlet and triplet intermediates, CPMCSCF/TZVPP optimized minimum-energy crossing point, including electronic states and point groups; CCSD/cc-pVTZ optimized geometries of the transition states for the $C(^3P) + SiH_4$ (X^1A_1) reaction on the adiabatic singlet and triplet ground-state potential energy surfaces; CCSD(T)/CBS energies with CCSD/cc-pVTZ zero-point energy corrections of CCSD/cc-pVTZ optimized reactants, intermediates, transition states, H, and H_2 dissociation products on the adiabatic triplet and singlet ground-state potential energy surfaces of $CSiH_4$; and CCSD/cc-pVTZ optimized Cartesian coordinates of intermediates, transition states, products, and CPMCSCF/TZVPP optimized minimum-energy crossing point on the triplet and singlet $CSiH_4$ potential energy surfaces (PDF)

■ AUTHOR INFORMATION

Corresponding Authors

Ralf I. Kaiser − *Department of Chemistry, University of Hawai'i at Manoa, Honolulu, Hawaii 96822, United States;* orcid.org/0000-0002-7233-7206; Email: ralfk@hawaii.edu

Agnes H. H. Chang − *Department of Chemistry, National Dong Hwa University, Shoufeng, Hualien 974, Taiwan;* Email: hhchang@gms.ndhu.edu.tw

Authors

Chao He − *Department of Chemistry, University of Hawai'i at Manoa, Honolulu, Hawaii 96822, United States*

Aaron M. Thomas − *Department of Chemistry, University of Hawai'i at Manoa, Honolulu, Hawaii 96822, United States;* orcid.org/0000-0001-8540-9523

Beni B. Dangi − *Department of Chemistry, University of Hawai'i at Manoa, Honolulu, Hawaii 96822, United States;* Present Address: Department of Chemistry, Florida Agricultural and Mechanical University, Tallahassee, FL 32307, United States; orcid.org/0000-0002-1866-8725

Tao Yang − *Department of Chemistry, University of Hawai'i at Manoa, Honolulu, Hawaii 96822, United States;* Present Address: State Key Laboratory of Precision Spectroscopy, East China Normal University, Shanghai, 200062, China.; orcid.org/0000-0003-4101-2385

Huan-Cheng Lee − *Department of Chemistry, National Dong Hwa University, Shoufeng, Hualien 974, Taiwan*

Bing-Jian Sun − *Department of Chemistry, National Dong Hwa University, Shoufeng, Hualien 974, Taiwan*

Complete contact information is available at: https://pubs.acs.org/10.1021/acs.jpca.2c01853

Notes

The authors declare no competing financial interest.

■ ACKNOWLEDGMENTS

These experiments were supported by the US National Science Foundation (CHE 1853541). Computer resources at the National Center for High-performance Computer of Taiwan were utilized in the calculations.

■ REFERENCES

(1) Millar, T. J. Chemistry in AGB Stars: Successes and Challenges. *J. Phys. Conf.* **2016**, *728*, 052001.

(2) Frenklach, M. Reaction Mechanism of Soot Formation in Flames. *Phys. Chem. Chem. Phys.* **2002**, *4*, 2028−2037.

(3) Frenklach, M.; Clary, D. W.; Gardiner, W. C., Jr.; Stein, S. E. Detailed Kinetic Modeling of Soot Formation in Shock-Tube Pyrolysis of Acetylene. *Symp. (Int.) Combust.* **1985**, *20*, 887−901.

(4) Parker, D. S. N.; Kaiser, R. I.; Troy, T. P.; Ahmed, M. Hydrogen Abstraction/Acetylene Addition Revealed. *Angew. Chem., Int. Ed.* **2014**, *53*, 7740−7744.

(5) Yang, T.; Troy, T. P.; Xu, B.; Kostko, O.; Ahmed, M.; Mebel, A. M.; Kaiser, R. I. Hydrogen-Abstraction/Acetylene-Addition Exposed. *Angew. Chem., Int. Ed.* **2016**, *55*, 14983−14987.
(6) Parker, D. S. N.; Zhang, F.; Kim, Y. S.; Kaiser, R. I.; Landera, A.; Kislov, V. V.; Mebel, A. M.; Tielens, A. G. G. M. Low Temperature Formation of Naphthalene and Its Role in the Synthesis of PAHs (Polycyclic Aromatic Hydrocarbons) in the Interstellar Medium. *Proc. Natl. Acad. Sci. U.S.A.* **2012**, *109*, 53−58.
(7) Zhao, L.; Kaiser, R. I.; Xu, B.; Ablikim, U.; Ahmed, M.; Joshi, D.; Veber, G.; Fischer, F. R.; Mebel, A. M. Pyrene Synthesis in Circumstellar Envelopes and Its Role in the Formation of 2D Nanostructures. *Nat. Astron.* **2018**, *2*, 413−419.
(8) Zhao, L.; Xu, B.; Ablikim, U.; Lu, W.; Ahmed, M.; Evseev, M. M.; Bashkirov, E. K.; Azyazov, V. N.; Howlader, A. H.; Wnuk, S. F.; et al. Gas-Phase Synthesis of Triphenylene ($C_{18}H_{12}$). *ChemPhysChem* **2019**, *20*, 791−797.
(9) Treffers, R.; Cohen, M. High-Resolution Spectra Of Cool Stars In The 10- and 20-Micron Regions. *Astrophys. J.* **1974**, *188*, 545−552.
(10) Yang, X.; Chen, P.; He, J. Molecular and Dust Features of 29 SiC Carbon AGB Stars. *Astron. Astrophys.* **2004**, *414*, 1049−1063.
(11) Zinner, E.; Nittler, L. R.; Gallino, R.; Karakas, A. I.; Lugaro, M.; Straniero, O.; Lattanzio, J. C. Silicon and Carbon Isotopic Ratios in AGB Stars: SiC Grain Data, Models, and the Galactic Evolution of the Si Isotopes. *Astrophys. J.* **2006**, *650*, 350.
(12) Davis, A. M. Stardust in Meteorites. *Proc. Natl. Acad. Sci. U.S.A.* **2011**, *108*, 19142−19146.
(13) Heck, P. R.; Greer, J.; Kööp, L.; Trappitsch, R.; Gyngard, F.; Busemann, H.; Maden, C.; Ávila, J. N.; Davis, A. M.; Wieler, R. Lifetimes of Interstellar Dust from Cosmic Ray Exposure Ages of Presolar Silicon Carbide. *Proc. Natl. Acad. Sci. U.S.A.* **2020**, *117*, 1884−1889.
(14) Boogert, A. C. A.; Gerakines, P. A.; Whittet, D. C. B. Observations of the Icy Universe. *Annu. Rev. Astron. Astrophys.* **2015**, *53*, 541−581.
(15) Kaiser, R. I.; Ochsenfeld, C.; Stranges, D.; Head-Gordon, M.; Lee, Y. T. Combined Crossed Molecular Beams and *Ab Initio* Investigation of the Formation of Carbon-bearing Molecules in the Interstellar Medium via Neutral−Neutral Reactions. *Faraday Discuss.* **1998**, *109*, 183−204.
(16) Remijan, A. J.; Snyder, L. E.; McGuire, B. A.; Kuo, H.-L.; Looney, L. W.; Friedel, D. N.; Golubiatnikov, G. Y.; Lovas, F. J.; Ilyushin, V. V.; Alekseev, E. A.; Dyubko, S. F.; McCall, B. J.; Hollis, J. M. Observational Results of a Multi-Telescope Campaign in Search of Interstellar Urea [$(NH_2)_2CO$]. *Astrophys. J.* **2014**, *783*, 77.
(17) Förstel, M.; Maksyutenko, P.; Jones, B. M.; Sun, B.-J.; Chang, A. H. H.; Kaiser, R. I. Synthesis of Urea in Cometary Model Ices and Implications for Comet 67P/Churyumov−Gerasimenko. *Chem. Commun.* **2016**, *52*, 741−744.
(18) Kaiser, R. I.; Maity, S.; Jones, B. M. Synthesis of Prebiotic Glycerol in Interstellar Ices. *Angew. Chem., Int. Ed.* **2015**, *54*, 195−200.
(19) Turner, A. M.; Bergantini, A.; Abplanalp, M. J.; Zhu, C.; Góbi, S.; Sun, B.-J.; Chao, K.-H.; Chang, A. H. H.; Meinert, C.; Kaiser, R. I. An Interstellar Synthesis of Phosphorus Oxoacids. *Nat. Commun.* **2018**, *9*, 3851.
(20) Förstel, M.; Bergantini, A.; Maksyutenko, P.; Góbi, S.; Kaiser, R. I. Formation of Methylamine and Ethylamine in Extraterrestrial Ices and Their Role as Fundamental Building Blocks of Proteinogenic α-Amino Acids. *Astrophys. J.* **2017**, *845*, 83.
(21) Holtom, P. D.; Bennett, C. J.; Osamura, Y.; Mason, N. J.; Kaiser, R. I. A Combined Experimental and Theoretical Study on the Formation of the Amino Acid Glycine (NH_2CH_2COOH) and Its Isomer ($CH_3NHCOOH$) in Extraterrestrial Ices. *Astrophys. J.* **2005**, *626*, 940.
(22) Muñoz Caro, G. M.; Meierhenrich, U. J.; Schutte, W. A.; Barbier, B.; Arcones Segovia, A.; Rosenbauer, H.; Thiemann, W. H.-P.; Brack, A.; Greenberg, J. M. Amino Acids from Ultraviolet Irradiation of Interstellar Ice Analogues. *Nature* **2002**, *416*, 403−406.
(23) Ligterink, N. F. W.; Terwisscha van Scheltinga, J.; Taquet, V.; Jørgensen, J. K.; Cazaux, S.; van Dishoeck, E. F.; Linnartz, H. The Formation of Peptide-Like Molecules on Interstellar Dust Grains. *Mon. Not. R. Astron. Soc.* **2018**, *480*, 3628−3643.
(24) Kaiser, R. I.; Stockton, A. M.; Kim, Y. S.; Jensen, E. C.; Mathies, R. A. On the Formation of Dipeptides in Interstellar Model Ices. *Astrophys. J.* **2013**, *765*, 111.
(25) Halfen, D. T.; Ilyushin, V.; Ziurys, L. M. Formation of Peptide Bonds in Space: a Comprehensive Study of Formamide and Acetamide in Sgr B2(N). *Astrophys. J.* **2011**, *743*, 60.
(26) Frigge, R.; Zhu, C.; Turner, A. M.; Abplanalp, M. J.; Bergantini, A.; Sun, B.-J.; Chen, Y.-L.; Chang, A. H. H.; Kaiser, R. I. A Vacuum Ultraviolet Photoionization Study on the Formation of N-Methyl Formamide ($HCONHCH_3$) in Deep Space: A Potential Interstellar Molecule with a Peptide Bond. *Astrophys. J.* **2018**, *862*, 84.
(27) Bernal, J. J.; Haenecour, P.; Howe, J.; Zega, T. J.; Amari, S.; Ziurys, L. M. Formation of Interstellar C_{60} from Silicon Carbide Circumstellar Grains. *Astrophys. J. Lett.* **2019**, *883*, L43.
(28) Cami, J.; Bernard-Salas, J.; Peeters, E.; Malek, S. E. Detection of C_{60} and C_{70} in a Young Planetary Nebula. *Science* **2010**, *329*, 1180−1182.
(29) Merino, P.; Švec, M.; Martinez, J. I.; Jelinek, P.; Lacovig, P.; Dalmiglio, M.; Lizzit, S.; Soukiassian, P.; Cernicharo, J.; Martin-Gago, J. A. Graphene Etching on SiC Grains as a Path to Interstellar Polycyclic Aromatic Hydrocarbons Formation. *Nat. Commun.* **2014**, *5*, 3054.
(30) Zhao, T. Q.; Li, Q.; Liu, B. S.; Gover, R. K. E.; Sarre, P. J.; Cheung, A. S.-C. Laboratory Astrochemistry: Catalytic Conversion of Acetylene to Polycyclic Aromatic Hydrocarbons over SiC Grains. *Phys. Chem. Chem. Phys.* **2016**, *18*, 3489−3496.
(31) Cernicharo, J.; Gottlieb, C. A.; Guelin, M.; Thaddeus, P.; Vrtilek, J. M. Astonomical and Laboratory Detection of the SiC Radical. *Astrophys. J.* **1989**, *341*, L25−L28.
(32) Ohishi, M.; Kaifu, N.; Kawaguchi, K.; Murakami, A.; Saito, S.; Yamamoto, S.; Ishikawa, S.-I.; Fujita, Y.; Shiratori, Y.; Irvine, W. M. Detection of a New Circumstellar Carbon Chain Molecule. C4Si. *Astrophys. J.* **1989**, *345*, L83−L86.
(33) Thaddeus, P.; Cummins, S. E.; Linke, R. A. Identification of the SiCC Radical Toward IRC +10216: The First Molecular Ring in an Astronomical Source. *Astrophys. J.* **1984**, *283*, L45−L48.
(34) Apponi, A. J.; McCarthy, M. C.; Gottlieb, C. A.; Thaddeus, P. Astronomical Detection of Rhomboidal SiC_3. *Astrophys. J.* **1999**, *516*, L103.
(35) Cernicharo, J.; McCarthy, M. C.; Gottlieb, C. A.; Agúndez, M.; Prieto, L. V.; Baraban, J. H.; Changala, P. B.; Guélin, M.; Kahane, C.; Drumel, M. A. M.; Patel, N. A.; Reilly, N. J.; Stanton, J. F.; Quintana-Lacaci, G.; Thorwirth, S.; Young, K. H. Discovery of SiCSi in IRC +10216: A Missing Link between Gas and Dust Carriers of Si−C Bonds. *Astrophys. J. Lett.* **2015**, *806*, L3.
(36) Guélin, M.; Muller, S.; Cernicharo, J.; Apponi, A. J.; McCarthy, M. C.; Gottlieb, C. A.; Thaddeus, P. Astronomical Detection of the Free Radical SiCN. *Astron. Astrophys.* **2000**, *363*, L9−L12.
(37) Agúndez, M.; Cernicharo, J.; Guélin, M. New Molecules in IRC +10216: Confirmation of C_5S and Tentative Identification of MgCCH, NCCP, and SiH_3CN. *Astron. Astrophys.* **2014**, *570*, A45.
(38) Cernicharo, J.; Agúndez, M.; Velilla Prieto, L.; Guélin, M.; Pardo, J. R.; Kahane, C.; Marka, C.; Kramer, C.; Navarro, S.; Quintana-Lacaci, G.; et al. Discovery of Methyl Silane and Confirmation of Silyl Cyanide in IRC + 10216. *Astron. Astrophys.* **2017**, *606*, L5.
(39) Massalkhi, S.; Agúndez, M.; Cernicharo, J.; Velilla Prieto, L.; Goicoechea, J. R.; Quintana-Lacaci, G.; Fonfría, J. P.; Alcolea, J.; Bujarrabal, V. Abundance of SiC_2 in Carbon Star Envelopes-Evidence that SiC_2 is a Gas-Phase Precursor of SiC Dust. *Astron. Astrophys.* **2018**, *611*, A29.
(40) Gobrecht, D.; Cristallo, S.; Piersanti, L.; Bromley, S. T. Nucleation of Small Silicon Carbide Dust Clusters in AGB Stars. *Astrophys. J.* **2017**, *840*, 117.

https://doi.org/10.1021/acs.jpca.2c01853
J. Phys. Chem. A 2022, 126, 3347−3357

(41) Cherchneff, I. The Inner Wind of IRC + 10216 Revisited: New Exotic Chemistry and Diagnostic for Dust Condensation in Carbon Stars. *Astron. Astrophys.* **2012**, *545*, A12.
(42) Agúndez, M.; Fonfría, J. P.; Cernicharo, J.; Kahane, C.; Daniel, F.; Guélin, M. Molecular Abundances in the Inner Layers of IRC + 10216. *Astron. Astrophys.* **2012**, *543*, A48.
(43) Goldhaber, D. M.; Betz, A. L. Silane in IRC + 10216. *Astrophys. J.* **1984**, *279*, L55−L58.
(44) Sakai, S.; Deisz, J.; Gordon, M. S. Theoretical Studies of the Insertion Reactions of Atomic Carbon and Silicon into Methane and Silane. *J. Phys. Chem.* **1989**, *93*, 1888−1893.
(45) Kim, G.-S.; Nguyen, T. L.; Mebel, A. M.; Lin, S. H.; Nguyen, M. T. Ab Initio/RRKM Study of the Potential Energy Surface of Triplet Ethylene and Product Branching Ratios of the $C(^3P) + CH_4$ Reaction. *J. Phys. Chem. A* **2003**, *107*, 1788−1796.
(46) Lu, I.-C.; Chen, W.-K.; Huang, W.-J.; Lee, S.-H. Dynamics of the Reaction $C(^3P) + SiH_4$: Experiments and Calculations. *J. Chem. Phys.* **2008**, *129*, 164304.
(47) Ranka, K.; Perera, A.; Bartlett, R. J. Elementary Reaction Profile and Chemical Kinetics Study of $[C(^1D)/(^3P) + SiH_4]$ with the CCSD(T) Method. *Chem. Phys. Lett.* **2017**, *680*, 61−68.
(48) Jones, B. M.; Zhang, F.; Kaiser, R. I.; Jamal, A.; Mebel, A. M.; Cordiner, M. A.; Charnley, S. B. Formation of Benzene in the Interstellar Medium. *Proc. Natl. Acad. Sci. U.S.A.* **2011**, *108*, 452−457.
(49) Guo, Y.; Gu, X.; Kawamura, E.; Kaiser, R. I. Design of a Modular and Versatile Interlock System for Ultrahigh Vacuum Machines: A Crossed Molecular Beam Setup as a Case Study. *Rev. Sci. Instrum.* **2006**, *77*, 034701.
(50) Gu, X.; Guo, Y.; Kawamura, E.; Kaiser, R. I. Characteristics and Diagnostics of an Ultrahigh Vacuum Compatible Laser Ablation Source for Crossed Molecular Beam Experiments. *J. Vac. Sci. Technol., A* **2006**, *24*, 505−511.
(51) Kaiser, R. I.; Sun, W.; Suits, A. G.; Lee, Y. T. Crossed Beam Reaction of Atomic Carbon, $C(^3P_j)$, with the Propargyl Radical, C_3H_3 (X^2B_2): Observation of Diacetylene, C_4H_2 ($X^1\Sigma_g^+$). *J. Chem. Phys.* **1997**, *107*, 8713−8716.
(52) Kaiser, R. I.; Hahndorf, I.; Huang, L. C. L.; Lee, Y. T.; Bettinger, H. F.; Schleyer, P. v. R.; Schaefer, H. F., III; Schreiner, P. R. Crossed Beams Reaction of Atomic Carbon, $C(^3P_j)$, with d_6-Benzene, C_6D_6 (X^1A_{1g}): Observation of the Per-deutero-1,2-didehydro-cyclo-heptatrienyl Radical, C_7D_5(X^2B_2). *J. Chem. Phys.* **1999**, *110*, 6091−6094.
(53) Kaiser, R. I.; Mebel, A. M.; Chang, A. H. H.; Lin, S. H.; Lee, Y. T. Crossed-Beam Reaction of Carbon Atoms with Hydrocarbon Molecules. V. Chemical Dynamics of n-C_4H_3 Formation from Reaction of $C(^3P_j)$ with Allene, H_2CCCH_2 (X^1A_1). *J. Chem. Phys.* **1999**, *110*, 10330−10344.
(54) Kaiser, R. I.; Stranges, D.; Bevsek, H. M.; Lee, Y. T.; Suits, A. G. Crossed-Beam Reaction of Carbon Atoms with Hydrocarbon Molecules. IV. Chemical Dynamics of Methylpropargyl Radical Formation, C_4H_5, from Reaction of $C(^3P_j)$ with Propylene, C_3H_6 (X^1A). *J. Chem. Phys.* **1997**, *106*, 4945−4953.
(55) Kaiser, R. I.; Lee, Y. T.; Suits, A. G. Crossed-Beam Reaction of $C(^3P_j)$ with $C_2H_2(^1\sum^+_g)$: Observation of Tricarbon-Hydride C_3H. *J. Chem. Phys.* **1995**, *103*, 10395−10398.
(56) Lucas, M.; Thomas, A. M.; Zhao, L.; Kaiser, R. I.; Kim, G.-S.; Mebel, A. M. Gas-Phase Synthesis of the Elusive Cyclooctatetraenyl Radical (C_8H_7) via Triplet Aromatic Cyclooctatetraene (C_8H_8) and Non-Aromatic Cyclooctatriene (C_8H_8) Intermediates. *Angew. Chem., Int. Ed.* **2017**, *56*, 13655−13660.
(57) Gu, X.; Guo, Y.; Zhang, F.; Mebel, A. M.; Kaiser, R. I. Reaction Dynamics of Carbon-bearing Radicals in Circumstellar Envelopes of Carbon Stars. *Faraday Discuss.* **2006**, *133*, 245−275.
(58) Huang, L. C. L.; Balucani, N.; Lee, Y. T.; Kaiser, R. I.; Osamura, Y. Crossed Beam Reaction of the Cyano Radical, $CN(X^2\Sigma^+)$, with Methylacetylene, CH_3CCH (X^1A_1): Observation of Cyanopropyne, CH_3CCCN (X^1A_1), and Cyanoallene, $H_2CCCHCN$ (X^1A'). *J. Chem. Phys.* **1999**, *111*, 2857−2860.
(59) Knowles, P. J.; Hampel, C.; Werner, H. J. Coupled Cluster Theory for High Spin, Open Shell Reference Wave Functions. *J. Chem. Phys.* **1993**, *99*, 5219−5227.
(60) Purvis, G. D., III; Bartlett, R. J. A Full Coupled-Cluster Singles and Doubles Model: The Inclusion of Disconnected Triples. *J. Chem. Phys.* **1982**, *76*, 1910−1918.
(61) Peterson, K. A.; Woon, D. E.; Dunning, T. H., Jr. Benchmark Calculations with Correlated Molecular Wave Functions. IV. The Classical Barrier Height of the $H+H_2 \rightarrow H_2+H$ Reaction. *J. Chem. Phys.* **1994**, *100*, 7410−7415.
(62) Peterson, K. A.; Dunning, T. H., Jr. Intrinsic Errors in Several Ab Initio Methods: the Dissociation Energy of N_2. *J. Phys. Chem.* **1995**, *99*, 3898−3901.
(63) Frisch, M. J.; Trucks, G. W.; Schlegel, H. B.; Scuseria, G. E.; Robb, M. A.; Cheeseman, J. R.; Scalmani, G.; Barone, V.; Mennucci, B.; Petersson, G. A.; et al. *Gaussian 09*, Revision A.1; Gaussian Inc.: Wallingford, CT, 2009; Vol. *200*, p 28.
(64) Werner, H.-J.; Knowles, P. J.; Lindh, R.; Manby, F. R.; Schütz, M.; Celani, P.; Korona, T.; Rauhut, G.; Amos, R. D.; Bernhardsson, A. *MOLPRO*, Version 2010.1, A Package of Ab Initio Programs; University of Cardiff: Cardiff: U.K., 2010.
(65) Mebel, A. M.; Kaiser, R. I. Formation of Resonantly Stabilised Free Radicals via the Reactions of Atomic Carbon, Dicarbon, and Tricarbon with Unsaturated Hydrocarbons: Theory and Crossed Molecular Beams Experiments. *Int. Rev. Phys. Chem.* **2015**, *34*, 461−514.
(66) Rettig, A.; Head-Gordon, M.; Doddipatla, S.; Yang, Z.; Kaiser, R. I. Crossed Beam Experiments and Computational Studies of Pathways to the Preparation of Singlet Ethynylsilylene (HCCSiH; X^1A'): The Silacarbene Counterpart of Triplet Propargylene (HCCCH; X^3B). *J. Phys. Chem. Lett.* **2021**, *12*, 10768−10776.
(67) Levine, R. D.; Bernstein, R. B.; Lee, Y. T. Molecular Reaction Dynamics and Chemical Reactivity. *Phys. Today* **1988**, *41*, 90−92.
(68) Miller, W. B.; Safron, S. A.; Herschbach, D. R. Exchange Reactions of Alkali Atoms with Alkali Halides: A Collision Complex Mechanism. *Discuss. Faraday Soc.* **1967**, *44*, 108−122.
(69) Levine, R. D. *Molecular Reaction Dynamics*; Cambridge University Press: Cambridge, 2005.
(70) Mandal, M.; Mahata, P.; Maiti, B. Importance of Intersystem Crossing in the $C(^3P) + SiH_4$ Reaction. *Phys. Chem. Chem. Phys.* **2020**, *22*, 8418−8426.
(71) Sansonetti, J. E.; Martin, W. C. Handbook of Basic Atomic Spectroscopic Data. *J. Phys. Chem. Ref. Data* **2005**, *34*, 1559−2259.
(72) Yang, T.; Dangi, B. B.; Kaiser, R. I.; Chao, K. H.; Sun, B. J.; Chang, A. H. H.; Nguyen, T. L.; Stanton, J. F. Gas-Phase Formation of the Disilavinylidene (H_2SiSi) Transient. *Angew. Chem., Int. Ed.* **2017**, *56*, 1264−1268.
(73) Thomas, A. M.; Dangi, B. B.; Yang, T.; Tarczay, G.; Kaiser, R. I.; Sun, B.-J.; Chen, S.-Y.; Chang, A. H. H.; Nguyen, T. L.; Stanton, J. F.; Mebel, A. M. Directed Gas-Phase Formation of the Germaniumsilylene Butterfly Molecule ($Ge(\mu$-$H_2)Si$). *J. Phys. Chem. Lett.* **2019**, *10*, 1264−1271.
(74) Sillars, D. S.; Bennett, C. J.; Osamura, Y.; Kaiser, R. I. Infrared Spectroscopic Detection of the Methylsilyl (CH_3SiH_2, X^2A') and the Silylmethyl (CH_2SiH_3, X^2A') Radicals and Their Partially Deuterated Counterparts in Low Temperature Matrices. *Chem. Phys.* **2005**, *315*, 41−52.
(75) Kaiser, R. I.; Osamura, Y. Laboratory Studies on the Infrared Absorptions of Hydrogenated Carbon-Silicon Clusters: Directing the Identification of Organometallic $SiCH_x$ Species Toward IRC + 10216. *Astrophys. J.* **2005**, *630*, 1217.
(76) Rappoport, Z.; Apeloig, Y. *Chemistry of organic silicon compounds*; John Wiley & Sons, 1998.
(77) Corey, J. Y. Historical Overview and Comparison of Silicon with Carbon. *Organic Silicon Compounds*; John Wiley & Sons, Ltd., 1989; Vol. *1*, pp 1−56.
(78) Sheldrick, W. S. Structural Chemistry of Organic Silicon Compounds. *Organic Silicon Compounds*; John Wiley & Sons, Ltd., 1989; Vol. *1*, pp 227−303.

https://doi.org/10.1021/acs.jpca.2c01853
J. Phys. Chem. A 2022, 126, 3347−3357